

ORIGINAL ARTICLE

ANO9 regulates PD-L2 expression and binding ability to PD-1 in gastric cancer

Keita Katsurahara¹  | Atsushi Shiozaki¹  | Toshiyuki Kosuga¹  | Hiroki Shimizu¹  |
 Michihiro Kudou¹  | Tomohiro Arita¹  | Hirotaka Konishi¹  | Shuhei Komatsu¹  |
 Takeshi Kubota¹  | Hitoshi Fujiwara¹  | Kazuma Okamoto¹  |
 Mitsuo Kishimoto²  | Eiichi Konishi²  | Eigo Otsuji¹ 

¹Division of Digestive Surgery, Department of Surgery, Kyoto Prefectural University of Medicine, Kyoto, Japan

²Department of Pathology, Kyoto Prefectural University of Medicine, Kyoto, Japan

Correspondence

Atsushi Shiozaki, Division of Digestive Surgery, Department of Surgery, Kyoto Prefectural University of Medicine, 465 Kajji-cho, Kamigyo-ku, Kyoto 602-8PD-L1566, Japan.

Email: shiozaki@koto.kpu-m.ac.jp

Funding information

Japan Society for the Promotion of Science, Grant/Award Number: 17K10602, 17K10710, 18K08628, 18K08689 and 19K09202

Abstract

The function of ANO9 in gastrointestinal cancer remains unclear. We investigated the biological behaviors and clinical prognostic values of ANO9 in gastric cancer (GC). Knockdown experiments were performed on human GC cell lines using ANO9 siRNA. Eighty-four primary tissue samples from patients with advanced GC were examined immunohistochemically (IHC). Knockdown of ANO9 reduced the progression of cancer cells in MKN7 and MKN74 cells. A microarray analysis revealed that ANO9 regulated PD-L2 via interferon (IFN)-related genes. We confirmed using flow cytometry that the depletion of ANO9 reduced the binding ability to PD-1 by downregulating the expression of PD-L2 in MKN7 and MKN74 cells. IHC revealed a correlation between the expression of ANO9 and PD-L2 and also that the strong expression of ANO9 was an independent poor prognostic factor in patients with advanced GC. The present results indicate that ANO9 regulates PD-L2 and binding ability to PD-1 via IFN-related genes in GC. Therefore, ANO9 has potential as a biomarker and target of immune checkpoint blockage (ICB) for GC.

KEYWORDS

ANO9, gastric cancer, immune checkpoint blockage, PD-1, PD-L2

1 | INTRODUCTION

The anoctamin family consists of transmembrane proteins in 10 isoforms and anoctamins (ANOs) are broadly expressed in epithelial and non-epithelial tissues.¹ ANOs mediate various functions, such as chloride ion transporters and phospholipid scramblase across the membrane.¹⁻⁸ These findings demonstrated that each subtype exhibits ion channel activity, scramblase activity, or both, however

these functions remain unclear. Anoctamin 9 (ANO9) was recently shown to be crucially involved in the progression of various cancers, such as colorectal cancer⁹ and pancreatic cancer.¹⁰ However, its contribution to the progression of gastric cancer (GC) and the clinical significance of its expression have not yet been examined in detail.

Programmed cell death 1 ligand 2 (PD-L2) is a cell surface protein that has been detected in some cancers including colorectal cancer,^{11,12} esophageal cancer,^{13,14} GC,^{15,16} hepatocellular carcinoma,^{17,18} breast

Keita Katsurahara and Atsushi Shiozaki contributed equally to this work.

This is an open access article under the terms of the Creative Commons Attribution-NonCommercial License, which permits use, distribution and reproduction in any medium, provided the original work is properly cited and is not used for commercial purposes.

© 2021 The Authors. Cancer Science published by John Wiley & Sons Australia, Ltd on behalf of Japanese Cancer Association.

cancer,¹⁹ and renal cell carcinoma²⁰ and regulates immune responses in cancer. Previous studies have suggested that programmed cell death 1 ligand 1 (PD-L1) was the only ligand for programmed cell death-1 (PD-1). However, PD-L2 has since been identified as a ligand for PD-1²¹ and is now attracting increasing attention as a new biomarker for immune checkpoint blockage (ICB) and as a therapeutic target.

We previously reported that several chloride ion channels and transporters played important roles in human GC. For example, intracellular chloride regulated cell proliferation²² and the cell cycle,^{23,24} and furosemide, a blocker of the Na⁺/K⁺/2Cl⁻ co-transporter, induced G₀/G₁ arrest,²⁵ while the blockade of chloride ion transport enhanced the cytotoxic effects of hypotonic solution.²⁶ In the present study, we focused on the expression of ANO9 in GC and investigated the function of ANO9 in the regulation of cancer growth using small interfering RNA (siRNA). The results obtained revealed a relationship between ANO9 and PD-L2 in the process of the functional analysis of ANO9. There is currently no evidence to show that ion transporters regulate PD-L2; therefore, we examined the effects of the knockdown of ANO9 on cancer immunity. We also investigated the expression of ANO9 and PD-L2 in GC tissue samples and analyzed its relationship between these genes and its prognostic impact in patients with GC.

2 | MATERIALS AND METHODS

2.1 | Cell lines, antibodies, and others

The GC cell lines MKN7, MKN45, MKN74, HGC27, and NUGC4 were purchased from the Riken Cell Bank. These cells were cultured in RPMI-1640 (Nacalai Tesque) supplemented with 100 µg/mL of streptomycin, 100 U/mL of penicillin, and 10% fetal bovine serum (FBS). Cells were cultured at 37°C in a 5% CO₂ incubator. The rabbit polyclonal anti-ANO9 antibody used in the immunohistochemical (IHC) analysis and western blotting was purchased from Abcam (ab140087). The rabbit polyclonal anti-PD-L2 antibody used in the IHC analysis was purchased from ProteinTech (18251-1-1AP). The mouse monoclonal anti-PD-L1 antibody was purchased from Cell Signaling Technology (#13684), the mouse monoclonal anti-CD8 antibody was purchased from Abcam (ab17147) and the mouse monoclonal anti-β-actin (ACTB) antibody was purchased from Sigma-Aldrich. Horseradish peroxidase (HRP)-conjugated anti-rabbit and mouse secondary antibodies were obtained from Cell Signaling Technology. We obtained PE anti-PD-L1 antibody (#329706) and APC anti-PD-L2 antibody (#329608) from Biolegends and recombinant human PD-1 (PE) from Abcam (ab246145). We purchased IFNα from EnoGene Biotechnology (E6L00101) and STAT3 inhibitor from Abcam (ab120952).

2.2 | Western blotting

Cells were washed twice with ice-cold PBS and lysed in M-PER buffer (Pierce) with protease inhibitors (Pierce). The modified Bradford

assay (Bio-Rad) was used to measure protein concentrations. Equal amounts of protein (10 mg/lane) were subjected to 10% SDS-PAGE gels and transferred to PVDF membranes (GE Healthcare), which were subsequently incubated with the indicated antibodies at 4°C for 24 h. An Amersham Imager 680 (GE Healthcare) was used to analyze band densities.

2.3 | Real-time reverse transcription-polymerase chain reaction (RT-PCR)

RNA was extracted from cancer cells using an RNeasy kit (Qiagen). A real-time quantitative PCR analysis was performed using the Step One plus Real-Time PCR System (Applied Biosystems) and TaqMan Gene Expression Assays (Applied Biosystems). PCR thermal cycle conditions were as follows: an initial step at 95°C for 10 min, followed by 40 cycles at 95°C for 15 s and at 60°C for 1 min. The expression levels of the following genes were assessed: ANO9 (Hs00947743_m1), PD-L1 (CD237) (Hs01125301_m1), PD-L2 (PDCD1LG2) (Hs01057777_m1), interferon (IFN) α-receptor1 (IFNAR1) (Hs01066116_m1), p21(CDKN1A) (Hs00355782_m1), JNK (MAPK8) (Hs01548508_m1), VIM (vimentin) (Hs00958111_m1), MMP2 (Hs00234422_m1), and MMP9 (Hs00234579_m1). The expression level of each gene was normalized to the housekeeping gene ACTB (Hs01060665_g1) (Applied Biosystems). Assays were performed in triplicate.

2.4 | siRNA transfection

Lipofectamine RNAiMAX reagent (Invitrogen) was used in all siRNA reverse transfection procedures at a final siRNA concentration of 24 nmol/L, as described by the manufacturer. ANO9 siRNA (Stealth RNAi™ siRNA #HSS179461) and control siRNA (Stealth RNAi™ siRNA Negative Control) were purchased from Invitrogen.

2.5 | Cell proliferation

Cells were seeded at a density of 0.8 × 10⁵ cells/well for MKN7 cells and 1.2 × 10⁵ cells/well for MKN74 cells on 6-well plates and incubated at 37°C in a 5% CO₂ in air incubator. siRNA was transfected at the same time as seeding. Cells were then detached from the plates using trypsin-EDTA 48 and 72 h after siRNA transfection and counted with a hemocytometer.

2.6 | Cell cycle assay

Cell cycle phases were assessed 48 h after siRNA transfection using flow cytometry with BD Accuri C6 (Becton-Dickinson Biosciences), as described by the manufacturer. Cells were detached from plates using trypsin-EDTA and treated with Triton X-100, and cell nuclei

were then stained with propidium iodide (PI) RNase staining buffer (BD Biosciences). The content of DNA was measured using flow cytometry with BD Accuri C6. At least 10 000 cells were analyzed.

2.7 | Apoptosis assay

Cells were evaluated 48 h after transfection and stained using the Annexin V-FITC Kit (Beckman Coulter). The proportion of early or late apoptotic cells was measured by flow cytometry with BD Accuri C6 (BD Biosciences), as described by the manufacturer. At least 10 000 cells were analyzed.

2.8 | Migration and invasion assays

A cell culture insert with 8- μ m pores (BD Biosciences) and 24-well plates were used in the migration assay, while the invasion assay was conducted with Biocoat Matrigel (BD Biosciences). At 48 h after siRNA transfection, MKN7 cells were seeded at a density of 1.0×10^5 cells/well and MKN74 cells at 2.0×10^5 cells/well into the upper chamber in RPMI-1640 (serum-free). The lower chamber contained RPMI-1640 with 10% FBS. After a 48-h incubation, any Matrigel and cells remaining in the upper chamber were removed. Migrated or invaded cells were stained using Diff-Quick staining reagents (Sysmex) and counted in 4 independent fields of view. Each assay was performed in triplicate.

2.9 | Microarray sample preparation

MKN7 cells were transfected with control siRNA and ANO9 siRNA, and total RNA was then extracted using a RNeasy kit (Qiagen). Cyanine 3 (Cy3)-labeled cRNA was prepared from 0.1 μ g total RNA using the Low Input Quick Amp Labeling Kit (Agilent Technologies), as described by the manufacturer, and then subjected to RNeasy column purification (Qiagen). Dye incorporation and cRNA yields were assessed using a NanoDrop ND-2000 spectrophotometer. A total of 0.6 μ g of Cy3-labeled cRNA was fragmented at 60°C for 30 min in a reaction volume of 25 μ L containing 1 \times Agilent fragmentation buffer and 2 \times Agilent blocking agent, as described by the manufacturer. After the fragmentation reaction, 25 μ L of 2 \times Agilent hybridization buffer was added to the fragmentation mixture and hybridized to SurePrint G3 Human GE 8x60K Microarray v.3.0 (Agilent Technologies) at 65°C for 17 h in a rotating Agilent hybridization oven. After hybridization, microarrays were washed at room temperature for 1 min with GE Wash Buffer 1 (Agilent Technologies) and at 37°C for 1 min with GE Wash Buffer 2 (Agilent Technologies).

2.10 | Microarray data processing

Slides were scanned on the Agilent SureScan Microarray Scanner (G2600D) using the one-color scan setting for 8 \times 60k array

slides. These images were then examined using Feature Extraction Software (Agilent Technologies) with the default parameters, and background-subtracted and spatially detrended Processed Signal intensities were obtained. Microarray data were investigated using Ingenuity Pathway Analysis (IPA) software (Ingenuity Systems, Inc).

2.11 | Surface PD-L1 /PD-L2 expression and binding ability to PD-1

Surface PD-L1 and PD-L2 expression were evaluated 48 h after siRNA transfection using flow cytometry with a BD Accuri C6 flow cytometer (BD Biosciences). Binding ability to PD-1 was assessed 48 h after siRNA transfection using flow cytometry with BD Accuri C6 (BD Biosciences). We applied recombinant human PD-1 (PE) according to the manufacturer's instructions. The experiment was performed 1 h after the application of these reagents. At least 10 000 cells were analyzed.

2.12 | Patients and primary tissue samples

Eighty-four patients with histologically confirmed primary advanced GC who underwent gastrectomy between 2011 and 2013 at Kyoto Prefectural University of Medicine were enrolled in the present study. Informed consent was provided by all patients prior to their enrollment. Patients who underwent non-curative resection or received preoperative chemotherapy were excluded. Twenty-one patients (25.0%) died in the follow-up period. The median follow-up time was 1743 d (range, 1081-2306 d). Patients were staged using the International Union Against Cancer (UICC)/TNM Classification of Malignant Tumors (8th edition).²⁷ The present study was approved by the Institutional Review Board of Kyoto Prefectural University of Medicine (ERB-C-1195).

2.13 | IHC

IHC staining was performed using the Vectastain ABC Elite Kit (Vector Laboratories) with the avidin-biotinylated peroxidase complex (ABC) method. Sections were deparaffinized in xylene and rehydrated in an ethanol series. Endogenous peroxidase activity in sections was blocked by an incubation in 0.3% H₂O₂ for 30 min. Endogenous biotin, biotin receptors, and avidin-binding sites were blocked using an Avidin/Biotin Blocking Kit (Vector Laboratories). Slides were then incubated with the ANO9 antibody (diluted 1:100) or PD-L2 antibody (diluted 1:100) at room temperature for 1 h and at 4°C overnight. Visualization was performed using a standard ABC method. Counterstaining was conducted with hematoxylin.

The semi-quantitative grading of IHC scores was performed based on staining intensities and the proportions of stained cancer cells. Staining intensity was scored as 0 (no staining), 1 (weak

staining), 2 (moderate staining), or 3 (strong staining). The proportion of stained cells was assessed as a percentage of the stained area in the cancer area and scored from 0 to 1.0. The IHC score of each sample was calculated as the maximum multiplied product of intensity and proportion scores (0-3.0).

2.14 | Statistical analysis

Categorical data were analyzed using the chi-squared test or Fisher exact test. Survival rates were estimated using the Kaplan-Meier method and survival curves were analyzed using the Log-rank test for equality. Prognostic factors for the multivariate analysis were identified using Cox proportional hazard model. Statistical analyses were

conducted using the statistical software JMP v.12 (SAS Institute Inc). Differences were considered to be significant when the P value was $<.05$.

3 | RESULTS

3.1 | ANO9 expression in GC cells

To evaluate ANO9 expression in GC, western blotting was performed on 5 human GC cell lines. The results showed that ANO9 was strongly expressed by MKN7 and MKN74 cells (Figure 1A). Knockdown experiments were performed using ANO9 siRNAs and the effects of the depletion of ANO9 on tumor progression were

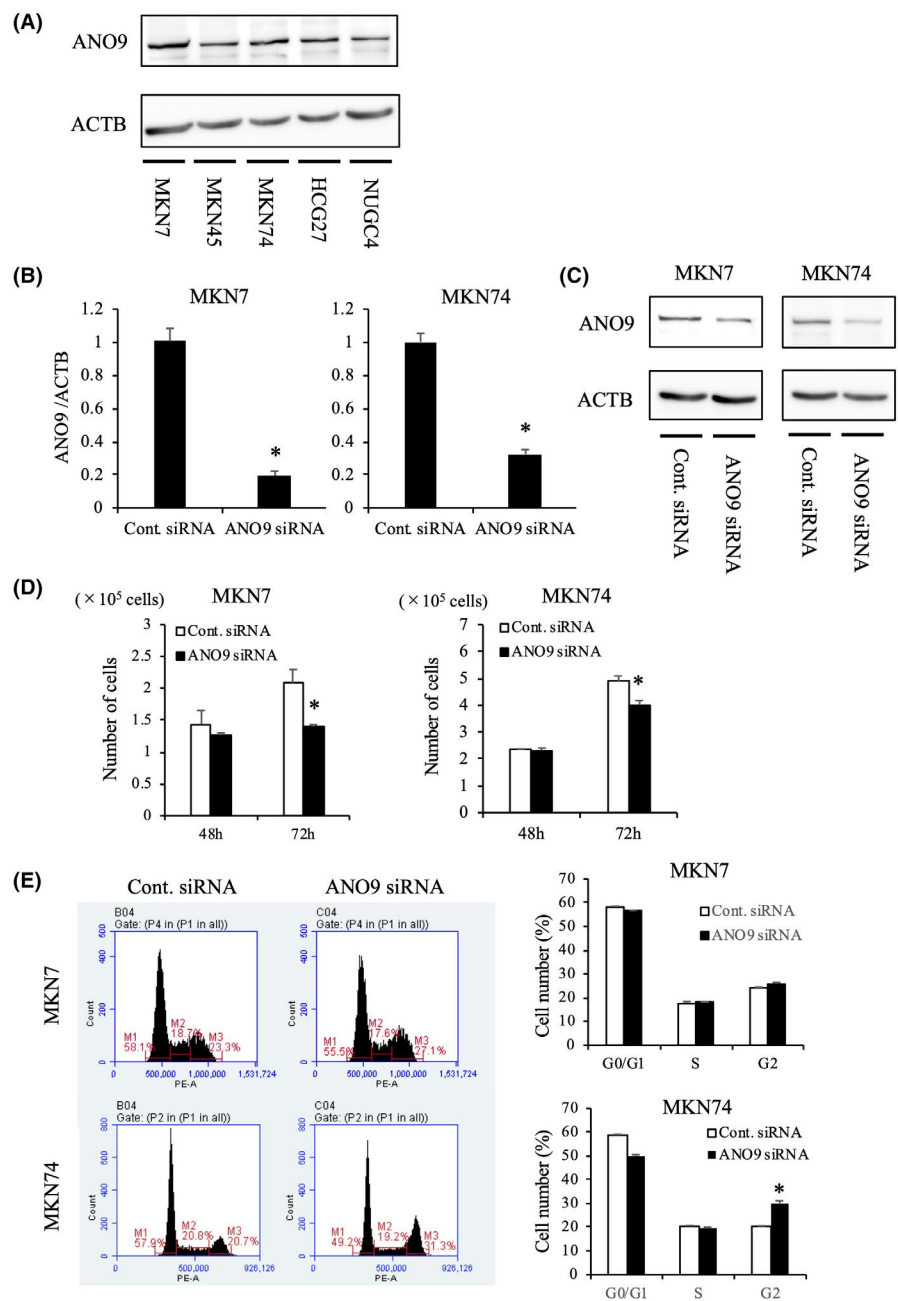


FIGURE 1 ANO9 controlled proliferation and the cell cycle in gastric cancer (GC) cells. A, Western blotting showed that ANO9 was strongly expressed in MKN7 and MKN74 cell lines in GC. B, Western blotting revealed that ANO9 siRNA effectively reduced ANO9 protein levels in MKN7 and MKN74 cells. C, ANO9 siRNA effectively reduced ANO9 mRNA levels in MKN7 and MKN74 cells. Mean \pm SEM. $n = 3$. $*P < .05$ (significantly different from control siRNA). D, Downregulation of ANO9 inhibited the proliferation of MKN7 and MKN74 cells. The number of cells was counted 48 and 72 h after siRNA transfection. Mean \pm SEM. $n = 3$. $*P < .05$ (significantly different from control siRNA). E, Downregulation of ANO9 increased the number of cells in the G₂/M phase in MKN7 and MKN74 cells. Cells transfected with control or ANO9 siRNA were stained with propidium iodide (PI) and analyzed by flow cytometry. Mean \pm SEM. $n = 3$. $*P < .05$ (significantly different from control siRNA)

examined using MKN7 and MKN74 cells. The knockdown of ANO9 using siRNA decreased ANO9 mRNA levels (Figure 1B) and ANO9 protein levels (Figure 1C) in MKN7 and MKN74 cells.

3.2 | ANO9 regulated cell proliferation and the cell cycle in GC cells

MKN7 and MKN74 cell numbers were significantly lower in ANO9 siRNA compared with in control siRNA 72 h after transfection (Figure 1D). Knockdown of ANO9 using siRNA reduced the percentage of G₂/M in MKN7 and MKN74 cells (Figure 1E). These results

indicated that ANO9 regulated the proliferation and cell cycle of GC cells.

3.3 | ANO9 regulated apoptosis in GC cells

Apoptosis assays on MKN7 and MKN74 cells with or without ANO9 siRNA were conducted to clarify the role of ANO9 in cell survival. The depletion of ANO9 significantly increased early apoptosis (annexin V-positive and PI-negative) and late apoptosis (annexin V-positive and PI-positive) in MKN7 and MKN74 cells 48 h after siRNA transfection (Figure 2A).

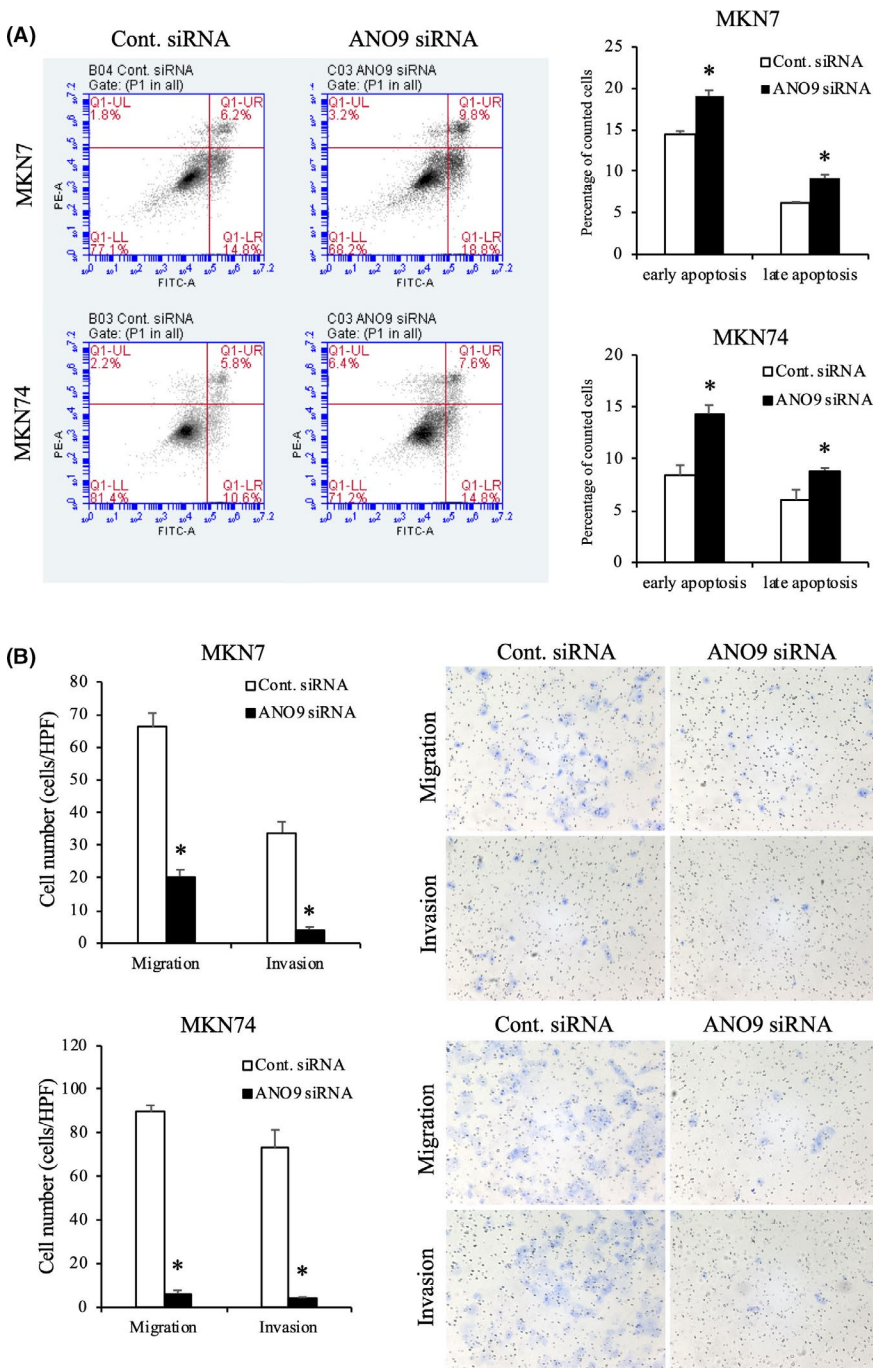


FIGURE 2 ANO9 controlled apoptosis, cell migration, and invasion in gastric cancer (GC) cells. A, Downregulation of ANO9 increased the early and late apoptosis phases in MKN7 and MKN74 cells. Cells transfected with control or ANO9 siRNA were stained with PI and annexin V, and then analyzed by flow cytometry. Mean \pm SEM. $n = 3$. * $P < .05$ (significantly different from control siRNA). B, Downregulation of ANO9 significantly reduced the migration and invasion of MKN7 and MKN74 cells. Cell migration and invasion were assessed by a Boyden chamber assay. Magnification: $\times 40$. Mean \pm SEM. $n = 3$. * $P < .05$ (significantly different from control siRNA)

3.4 | Depletion of ANO9 reduced cell migration and invasion in GC cells

We performed knockdown experiments on MKN7 and MKN74 cells with ANO9 siRNA and investigated the effects of the ANO9 knockdown on cell migration and invasion using a Boyden chamber assay. The depletion of ANO9 significantly reduced cell migration and invasion in MKN7 and MKN74 cells (Figure 2B).

3.5 | Gene expression profiling in ANO9 siRNA-transfected MKN7 cells

The gene expression profiles of ANO9-depleted MKN7 cells were examined using a microarray analysis. Fold changes of >2.7 were observed in the expression of 869 genes following the knockdown of ANO9 in MKN7 cells. Among these genes, 417 were upregulated and 452 were downregulated. The 20 genes showing the greatest increases and decreases in expression levels in ANO9-depleted MKN7 cells are shown in Table S1. IPA identified "Connective Tissue Disorders," "Inflammatory Disease," and "Inflammatory Response" as 3 of the top-ranked diseases and disorders associated with the depletion of ANO9 (Table S2). "Lymphoid Tissue Structure and Development, Antimicrobial Response, Inflammatory Response" was the fifth in the top networks. These results indicated that ANO9 regulated immune-related functions in GC cells.

3.6 | ANO9 regulated cancer progression

When the fold change was set to 1.4, the results of the microarray analysis showed that ANO9 regulated the STAT3 pathway (Figure S1A). In order to confirm the results of the microarray analysis, JNK and p21 expression in MKN7 and MKN74 were validated using quantitative RT-PCR (Figure S1B).

We performed proliferation assay and migration and invasion assay with STAT3 inhibitor (50 μ M, 24 h after transfection). As a result, STAT3 inhibitor tended to suppress the proliferation inhibitory effect of ANO9 siRNA in MKN7 and MKN74 cells (Figure S2A), and suppressed the cell migration and invasion effect of ANO9 siRNA in MKN7 and MKN74 cells (Figure S2B).

We extracted mesenchymal markers from microarray data to investigate the mechanism of regulating cell migration and invasion. Downregulation of mesenchymal markers such as VIM, MMP2, and MMP9 were observed (Table S3). In order to confirm the results of the microarray analysis, VIM, MMP2, and MMP9 expression in MKN7 and MKN74 were validated using quantitative RT-PCR (Figure S3).

3.7 | ANO9 regulated immune-related functions

We focused on the "Lymphoid Tissue Structure and Development, Antimicrobial Response, Inflammatory Response" networks of

ANO9 functions in the microarray analysis (Table S2, Figure 3A). In the network, PD-L2 (PDCD1LG2 in Figure 3A) was regulated from the interferon alpha receptor (IFNAR) and IFN α . To provide further evidence to support the results of the microarray analysis, we evaluated IFNAR and PD-L2 using quantitative RT-PCR (Figure 3B).

Knockdown of ANO9 did not affect the mRNA expression of PD-L1, but decreased that of PD-L2 (Figure 4A). Knockdown of ANO9 decreased surface PD-L2 expression in MKN7 and MKN74 cells (Figure S4). We evaluated binding ability to PD-1 using recombinant PD-1 (PE). ANO9-depleted cells showed significantly less binding for PD-1 in MKN7 and MKN74 (Figure 4B).

We also evaluated PD-L1, PD-L2, and binding ability to PD-1 under the condition with IFN α (100 U/mL for 24 h). In MKN7 cells, the addition of IFN α increased the mRNA expression of PD-L1 and PD-L2, but knockdown of ANO9 suppressed the increase in mRNA expression of PD-L2 when IFN α was added (Figure S5A). Similarly, surface expression was also attenuated in PD-L2 (Figure S5B). In addition, knockdown of ANO9 suppressed the enhancement of the binding ability to PD-1 when IFN α was added (Figure S5C). Similar changes were observed under the condition with IFN α in MKN74 cells (Figure S6).

3.8 | IHC analysis of ANO9, PD-L2, and PD-L1 expression in GC tissues

IHC showed that ANO9 was expressed in the epithelia of non-cancer tissue (Figure 5A) and cancer (Figure 5B), and PD-L2 was also expressed in the epithelia of non-cancer tissue (Figure 5F) and cancer (Figure 5G). Low expression cases of ANO9 are shown in Figure 5C and PD-L2 in Figure 5H, while high expression cases of ANO9 are shown in Figure 5D and PD-L2 in Figure 5I. The median score of ANO9 expression was 1.9 (range = 1.5-2.3) and the mean score of ANO9 expression was 1.89 (standard deviation (SD) = 0.55). The median score of PD-L2 expression was 1.4 (range = 0.9-2.0) and the mean score of PD-L2 expression was 1.35 (standard deviation (SD) = 0.69). We compared ANO9 and PD-L2 scores and found that these IHC scores correlated in each case ($P < .001$, $R^2 = 0.356$) (Figure 5K), and their tissue distribution was often similar. We validated the reactivity as a specific reaction to PD-L2 using monoclonal antibody (TA808982; OriGene Technologies; Figure S7).

Cut-off values were selected to obtain the smallest P -values in comparisons of 5-y overall survival (OS) rates between the 2 groups. The 5-y OS rates with each cut-off value are shown in Table S4. Patients were divided into low ANO9 expression (ANO9 scores < 1.8 , $n = 53$) and high ANO9 expression groups (ANO9 scores ≥ 1.8 , $n = 31$) (Figure 5E) and low PD-L2 expression (PD-L2 scores < 1.5 , $n = 60$) and high PD-L2 expression groups (PD-L2 scores ≥ 1.5 , $n = 24$) based on cut-off values (Figure 5J). In the analysis of clinicopathological features, ANO9 expression correlated with tumor length, histological type, and pathological T stage (Table S5),

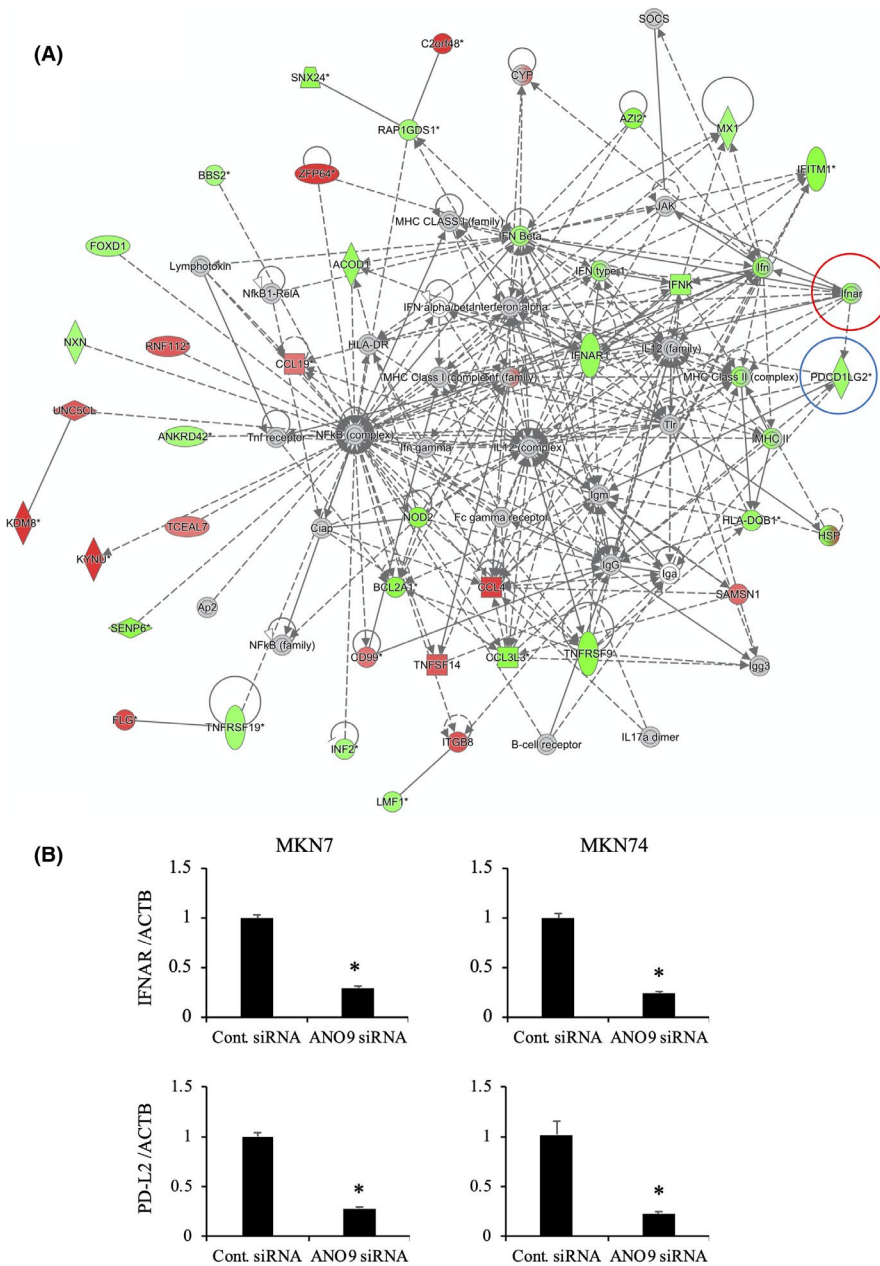


FIGURE 3 Network analyses by Ingenuity Pathway Analysis in ANO9-depleted MKN7 cells. A, “Inflammatory Response” was one of the top-ranked networks related to the knockdown of ANO9 cells according to Ingenuity Pathway Analysis. Red and green colors indicate genes with expression levels that were higher or lower, respectively, compared with reference RNA levels. A red circle was drawn in PDCD1LG2 (PD-L2) and a blue circle was drawn in IFNAR. B, Verification of gene expression by real-time quantitative RT-PCR. Expression levels of IFNAR and PD-L2 in ANO9-depleted MKN7 and MKN74 cells were compared with those in control siRNA-transfected cells using real-time quantitative RT-PCR. Mean \pm SEM. $n = 3$. * $P < .05$ (significantly different from control siRNA)

whereas PD-L2 expression did not (Table S6). We investigated the prognostic significance of ANO9 and PD-L2 expression after curative resection. We compared the following 12 variables: gender, age, tumor length, Borrmann type, histological differentiation, lymphatic invasion, venous invasion, pathological T stage, pathological N stage, and ANO9 and PD-L2 expression. The univariate analysis showed that the tumor length, Borrmann type, lymphatic invasion, pathological T stage, pathological N stage, and ANO9 and PD-L2 expression categories correlated with prognosis ($P = .045, <.0001, .006, .018, .004, <.0001, \text{ and } .015$, respectively). The multivariate analysis identified high ANO9 expression (≥ 1.8) and Borrmann type4 as an independent prognostic factor in patients with GC ($P = .045$ and $.014$, respectively) (Table 1).

We also performed IHC analysis for PD-L1 in our GC cohort (Figure S8A-D) and most cases were PD-L1 negative. The median

score of PD-L1 expression was 0.5 (range = 0.0-1.0) and the mean score of PD-L1 expression was 0.60 (standard deviation (SD) = 0.59). IHC score of PD-L1 was not associated to ANO9 expression ($P = .183, R^2 = 0.022$) (Figure S8E), and not correlated with prognosis in patients with GC ($P = .955$) (Figure S8F).

4 | DISCUSSION

ANO9 is also known as transmembrane protein 16J (TMEM16J) and is expressed in the human nasal and colonic epithelia, as well as in the respiratory, digestive, skeletal, and integumentary systems, during development.²⁸ ANO9 was also found to be expressed in human colorectal, lung, and breast cancers *in silico*.²⁹ However, its biological functions and clinical relevance in cancer currently remain unknown.

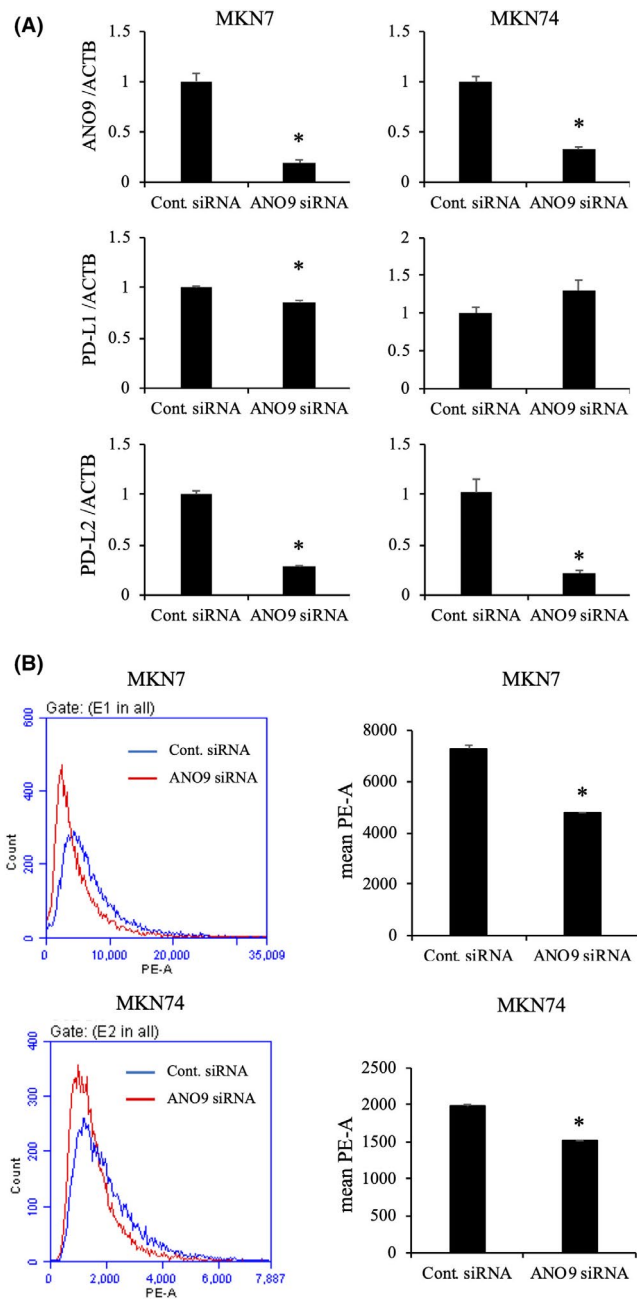


FIGURE 4 Binding ability to PD-1 in ANO9-depleted gastric cancer (GC) cells. A, Verification of gene expression by real-time quantitative RT-PCR. Expression levels of genes (ANO9, PD-L1, and PD-L2) in ANO9-depleted MKN7 and MKN74 cells were compared with those in control siRNA-transfected cells using real-time quantitative RT-PCR. Mean \pm SEM. $n = 3$. * $P < .05$ (significantly different from control siRNA). B, Downregulation of ANO9 reduced binding ability to PD-1 in MKN7 and MKN74 cells. Cells transfected with control or ANO9 siRNA and stained with recombinant PD-1 were analyzed by flow cytometry. Mean \pm SEM. $n = 3$. * $P < .05$ (significantly different from control siRNA)

Previous studies have reported that ANO9 regulated cancer growth via the epidermal growth factor receptor (EGFR) signaling pathway in pancreatic cancer. Regarding the other isoforms of ANOs, ANO1 regulated the PI3K/Akt signaling pathway in ovarian cancer,³⁰ the

EGFR signaling pathway in head and neck cancer,³¹ and the TNF α signaling pathway in prostate cancer.³²

In the present study, tumor suppressive effects were observed following the knockdown of ANO9, such as decreased proliferation, increased apoptosis, and less migration and invasion. A microarray analysis was performed to elucidate why these effects occurred. The results of the microarray analysis showed that ANO9 regulated the STAT3 pathway (Figure S1). STAT3 inhibitor reduced the effect of ANO9 siRNA in proliferation assay and migration and invasion assay (Figure S2).

Following the microarray analysis, we focused on PD-L2, which was previously reported to regulate cancer-associated immune responses, however the mechanisms regulating PD-L2 in GC remain unclear. PD-L1 is widely expressed by tumor cells and may be regulated by proinflammatory cytokines, such as IFN.³³ Conversely, the role of PD-L2 expressed in tumor cells has paid less attention and has been considered less relevant in predicting responses to ICB. But, PD-L2 binds to PD-1 with a higher (2- to 6-fold) affinity as compared to PD-L1,³³ and has potential as a biomarker and therapeutic target of ICB.

In the present study, PD-L2 and IFN-related genes were identified in the network analysis. IFN was reported the most important signal for the expression of PD-L1 and PD-L2.³⁴ And, it was reported that IFN α derived from DC and tumor cells promote tumor eradication.³⁵ This is the first study to show that ANO9 is further upstream of PD-L2 and IFNAR. In the present study, IFN α reduced the effect of ANO9 siRNA in PD-L2 expression (Figures S5 and S6). These results support the hypothesis that ANO9 regulated PD-L2 via IFN α .

Over the past decade, one of the most important breakthroughs in cancer treatment has been ICB of PD-1. PD-L1 expression, mismatch repair deficiency,³⁶ microsatellite instability,³⁷ and infiltrating CD8⁺ T cells in cancer tissue³⁸ were identified as predictive biomarkers for ICB in several cancers. Furthermore, combined positive score (CPS), which takes into account the PD-L1 positivity on cancer and infiltrating immune cells, are adopted in GC³⁹, however this remains controversial.

There are cases for which ICB is effective, even with the weak expression of PD-L1, and these cases are considered to be related to PD-L2. Therefore, PD-L2 is attracting increasing attention as a biomarker for ICB and as a therapeutic target. We confirmed that binding ability to PD-1 in ANO9-depleted cells was significantly decreased due to the downregulation of PD-L2, but not PD-L1, in MKN7 and MKN74 cells. These results indicated that PD-L2 suppresses the immune escape of cancer cells via PD-1 by the knockdown of ANO9. These results indicated that ANO9 and PD-L2 may be more effective biomarkers when we combine with conventional biomarkers.

The strong expression of ANO9 in IHC was previously shown to be associated with a poor prognosis in pancreatic cancer¹⁰ and good prognosis in colorectal cancer⁹, however its relationship with GC remains unclear. Regarding the other isoforms of ANOs, ANO1 was associated with a poor prognosis in esophageal squamous cell

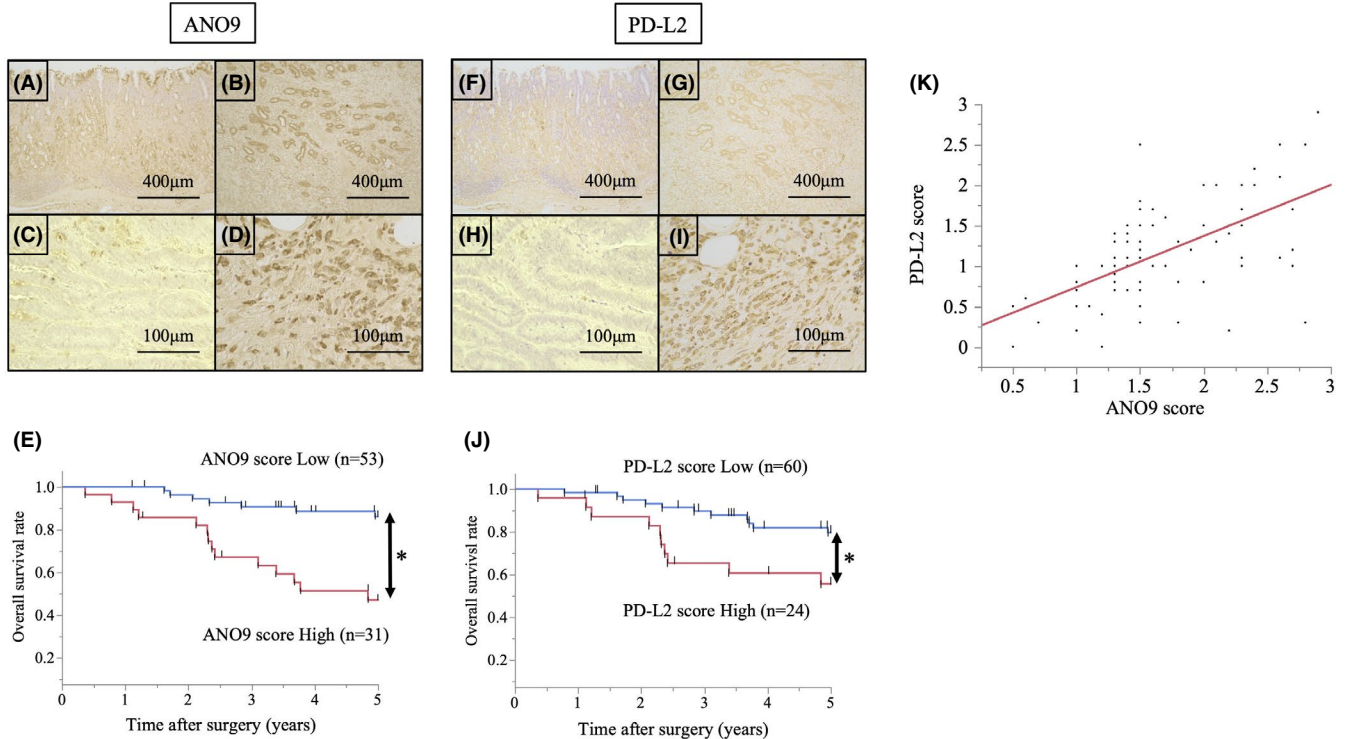


FIGURE 5 IHC analysis of human gastric cancer (GC) tissue. A, IHC staining of non-cancerous gastric epithelia with the ANO9 antibody. Magnification: $\times 100$. B, IHC staining of primary human GC samples with the ANO9 antibody. Magnification: $\times 100$. The IHC of ANO9 are results shown with low expression (C) and high expression (D). Magnification: $\times 400$. E, All patients were classified into 2 groups: a low ANO9 expression group (< 1.8 , $n = 53$, blue line) and high ANO9 expression group (≥ 1.8 , $n = 31$, red line). * $P < .05$ (significant difference). F, IHC staining of non-cancerous gastric epithelia with the PD-L2 antibody. Magnification: $\times 100$. G, IHC staining of primary human GC samples with the ANO9 antibody. Magnification: $\times 100$. IHC of PD-L2 shows low expression (H) and high expression (I). Magnification: $\times 400$. J, All patients were classified into 2 groups: a low PD-L2 expression group (< 1.5 , $n = 60$, blue line) and high PD-L2 expression group (≥ 1.5 , $n = 24$, red line). * $P < .05$ (significant difference). K, Scatter plot comparing the IHC score between ANO9 and PD-L2 in gastric cancer tissue. An approximately straight line was drawn

carcinoma⁴⁰ and lung cancer⁴¹ and a good prognosis in breast cancer.⁴² As we found a correlation between ANO9 and PD-L2 in an in vitro study, we compared them in an IHC analysis. PD-L2 was previously reported to be a poor prognostic factor based on IHC in hepatocellular carcinoma,¹⁷ esophageal cancer,⁴³ and colorectal cancer⁴⁴ and has also been suggested as a biomarker. Although PD-L2 has not yet been examined in detail, it was identified as a poor prognosis factor in GC by IHC.¹⁶

We examined the relationship between ANO9 and PD-L2 protein expression in GC tissue using IHC. The IHC scores of ANO9 and PD-L2 correlated in each case, and their distribution in tissue was often similar. Meanwhile, IHC score of PD-L1 was low and not associated with ANO9 expression in GC. These results support the hypothesis that ANO9 regulates PD-L2 expression in vitro. Furthermore, ANO9 was identified as an independent poor prognostic factor when a survival analysis was performed by combining these IHC scores with clinicopathological factors. This is the first study to show that the expression of ANO9 and PD-L2 correlated in cancer tissue and that the strong expression of ANO9 in an IHC analysis was a novel prognostic factor in patients with GC.

Furthermore, we performed IHC for CD8 in GC samples. As a result, ANO9 and PD-L2 expression were inversely associated with

CD8 T cell infiltration (Figure S9). These results support the hypothesis that ANO9 regulates the immune microenvironment via PD-L2 expression in GC.

The limitation of the present study is that various external factors, such as *H. pylori* and Epstein-Barr virus (EBV) virus infection, affect the carcinogenesis and growth of GC, but were not considered. A correlation has been reported between PD-L1 expression and EBV⁴⁵ and needs to be considered in the mechanisms contributing to cancer immunity, however it was not possible to collect this information in the present study. Future research is warranted. Secondly, it was found that knockdown of ANO9 attenuated the increase in PD-L2 expression when IFN α was added. Conversely, PD-L1 increased when IFN α was added (Figures S5 and S6). cBioPortal analyses of The Cancer Genome Atlas (TCGA) gene expression database (TCGA PanCancer Atlas) showed the correlation of PD-L2 and IFNAR rather than PD-L1 and IFNAR in GC samples (Spearman correlation coefficient was 0.20, $P < .001$, Spearman correlation coefficient was 0.10, $P = .037$, respectively) (Figure S10). These data from TCGA database that PD-L2 had a strong correlation with IFNAR may support our results, and further research is needed in the future.

TABLE 1 A 5-y overall survival rate of patients with gastric cancer according to various clinicopathological parameters

Variables	n	5-y OS	Univariate	Multivariate		
			P value*	95% CI	HR	P value**
Total	84					
Gender						
Male	61	74.9%	.575			
Female	23	68.5%				
Age						
<70	45	81.3%	.067			
≥70	39	62.5%				
Location						
U	27	70.5%	.658			
M,L	57	74.1%				
Tumor length						
<40	23	89.8%	.045*	0.26-5.49	1.19	.542
≥40	61	66.8%				
Borrmann type						
Type 4	9	22.2%	<.0001*	1.30-10.33	3.67	.014**
Other type	75	79.5%				
Histological type						
Differentiated	41	74.5%	.685			
Undifferentiated	43	71.2%				
Lymphatic invasion						
Negative	30	93.0%	.006*	0.66-17.10	3.37	.143
Positive	54	61.7%				
Venous invasion						
Negative	35	69.4%	.673			
Positive	49	75.7%				
pT						
pT2	26	91.7%	.018*	0.53-10.73	2.38	.260
pT3-4	58	64.7%				
pN						
pN0	43	89.8%	.0004*	0.52-6.67	1.86	.344
pN1-3	41	54.6%				
ANO9 score						
<1.8	53	87.3%	<.0001*	1.02-8.25	2.91	.045**
≥1.8	31	49.1%				
PD-L2 score						
<1.5	60	79.6%	.015*	0.64-4.31	1.67	.293
≥1.5	24	55.6%				

Note: pN, pathological N stage; pT, pathological T stage.

* $P < .05$: Log-rank test.

** $P < .05$: Cox's hazard regression analysis; HR: hazard ratio.

In summary, ANO9 promotes cancer growth via the STAT3 pathway and regulates PD-L2 expression via IFN-related genes in GC. When PD-L2 decreased under the control from ANO9, the binding ability of cancer cells to PD-1 decreased, which may have prevented immune escape. In the IHC analysis, a correlation was observed

between the expression of ANO9 and PD-L2, and the strong expression of ANO9 was an independent poor prognostic factor in GC. Although further studies are needed, the results of the present study indicated that ANO9 has potential as a biomarker and therapeutic target of ICB for GC.

ACKNOWLEDGMENTS

This work was supported by Grants-in-Aid for Scientific Research (C) (17K10602, 17K10710, 18K08628, 18K08689, and 19K09202) from the Japan Society for the Promotion of Science.

CONFLICT OF INTEREST

The authors declare that they have no competing interests.

AUTHOR CONTRIBUTIONS

AS, KK, MK, EK, EO designed the research; AS, KK, and EO wrote the paper; KK performed cell culture, molecular biology, and several experiments; TK, HS, MK, TA, HK, SK, TK, HF, KO, and EO provided clinical specimens and performed clinical data analyses.

ETHICAL STATEMENT

All procedures followed were in accordance with the ethical standards of the responsible committee on human experimentation (institutional and national) and with the Declaration of Helsinki 1964 and later versions. Informed consent to be included in the study, or the equivalent, was obtained from all patients.

DATA AVAILABILITY STATEMENT

The data sets used and analyzed during the current study are available from the corresponding author on reasonable request.

ORCID

Keita Katsurahara  <https://orcid.org/0000-0002-4841-497X>
 Atsushi Shiozaki  <https://orcid.org/0000-0003-3739-160X>
 Toshiyuki Kosuga  <https://orcid.org/0000-0002-1657-7272>
 Hiroki Shimizu  <https://orcid.org/0000-0002-6463-8498>
 Michihiro Kudou  <https://orcid.org/0000-0003-3518-528X>
 Tomohiro Arita  <https://orcid.org/0000-0001-7127-6504>
 Hirotaka Konishi  <https://orcid.org/0000-0002-4899-8944>
 Shuhei Komatsu  <https://orcid.org/0000-0001-6074-7614>
 Takeshi Kubota  <https://orcid.org/0000-0002-2246-3028>
 Hitoshi Fujiwara  <https://orcid.org/0000-0002-6507-4313>
 Kazuma Okamoto  <https://orcid.org/0000-0002-8270-4217>
 Mitsuo Kishimoto  <https://orcid.org/0000-0002-7407-9044>
 Eiichi Konishi  <https://orcid.org/0000-0002-1194-1186>
 Eigo Otsuji  <https://orcid.org/0000-0002-3260-8155>

REFERENCES

- Schreiber R, Uliyakina I, Kongsuphol P, et al. Expression and function of epithelial anoctamins. *J Biol Chem*. 2010;285:7838-7845.
- Brunner JD, Schenck S, Dutzler R. Structural basis for phospholipid scrambling in the TMEM16 family. *Curr Opin Struct Biol*. 2016;39:61-70.
- Kunzelmann K. TMEM16, LRRC8A, bestrophin: chloride channels controlled by Ca(2+) and cell volume. *Trends Biochem Sci*. 2015;40:535-543.
- Wanitchakool P, Wolf L, Koehl GE, et al. Role of anoctamins in cancer and apoptosis. *Philos Trans R Soc Lond B Biol Sci*. 2014;369:20130096.
- Pedemonte N, Galletta LJ. Structure and function of TMEM16 proteins (anoctamins). *Physiol Rev*. 2014;94:419-459.
- Kunzelmann K, Tian Y, Martins JR, et al. Anoctamins. *Pflugers Arch*. 2011;462:195-208.
- Kunzelmann K, Kongsuphol P, Chootip K, et al. Role of the Ca²⁺-activated Cl⁻ channels bestrophin and anoctamin in epithelial cells. *Biol Chem*. 2011;392:125-134.
- Kunzelmann K, Kongsuphol P, Aldehni F, et al. Bestrophin and TMEM16-Ca(2+) activated Cl(-) channels with different functions. *Cell Calcium*. 2009;46:233-241.
- Li C, Cai S, Wang X, Jiang Z. Identification and characterization of ANO9 in stage II and III colorectal carcinoma. *Oncotarget*. 2015;6:29324-29334.
- Jun I, Park HS, Piao HE, et al. ANO9/TMEM16J promotes tumorigenesis via EGFR and is a novel therapeutic target for pancreatic cancer. *Br J Cancer*. 2017;117:1798-1809.
- Guo PD, Sun ZW, Lai HJ, et al. Clinicopathological analysis of PD-L2 expression in colorectal cancer. *Onco Targets Ther*. 2018;11:7635-7642.
- Masugi Y, Nishihara R, Hamada T, et al. Tumor PDCD1LG2 (PD-L2) expression and the lymphocytic reaction to colorectal cancer. *Cancer Immunol Res*. 2017;5:1046-1055.
- Hsieh CC, Hsu HS, Li AF, Chen YJ. Clinical relevance of PD-L1 and PD-L2 overexpression in patients with esophageal squamous cell carcinoma. *J Thorac Dis*. 2018;10:4433-4444.
- Derks S, Nason KS, Liao X, et al. Epithelial PD-L2 expression marks Barrett's esophagus and esophageal adenocarcinoma. *Cancer Immunol Res*. 2015;3:1123-1129.
- Lingohr P, Dohmen J, Semaan A, et al. Clinicopathological, immune and molecular correlates of PD-L2 methylation in gastric adenocarcinomas. *Epigenomics*. 2019;11:639-653.
- Gao Y, Li SU, Xu D, et al. Prognostic value of programmed death-1, programmed death-ligand 1, programmed death-ligand 2 expression, and CD8(+) T cell density in primary tumors and metastatic lymph nodes from patients with stage T1-4N+M0 gastric adenocarcinoma. *Chin J Cancer*. 2017;36:61.
- Jung HI, Jeong D, Ji S, et al. Overexpression of PD-L1 and PD-L2 is associated with poor prognosis in patients with hepatocellular carcinoma. *Cancer Res Treat*. 2017;49:246-254.
- Xu P, Sun Z, Wang Y, Miao C. Long-term use of indomethacin leads to poor prognoses through promoting the expression of PD-1 and PD-L2 via TRIF/NF-kappaB pathway and JAK/STAT3 pathway to inhibit TNF-alpha and IFN-gamma in hepatocellular carcinoma. *Exp Cell Res*. 2015;337:53-60.
- Baptista MZ, Sarian LO, Derchain SF, Pinto GA, Vassallo J. Prognostic significance of PD-L1 and PD-L2 in breast cancer. *Hum Pathol*. 2016;47:78-84.
- Erlmeier F, Weichert W, Autenrieth M, et al. PD-L2: A prognostic marker in chromophobe renal cell carcinoma? *Med Oncol*. 2017;34:71.
- Latchman Y, Wood CR, Chernova T, et al. PD-L2 is a second ligand for PD-1 and inhibits T cell activation. *Nat Immunol*. 2001;2:261-268.
- Ohsawa R, Miyazaki H, Niisato N, et al. Intracellular chloride regulates cell proliferation through the activation of stress-activated protein kinases in MKN28 human gastric cancer cells. *J Cell Physiol*. 2010;223:764-770.
- Shiozaki A, Otsuji E, Marunaka Y. Intracellular chloride regulates the G(1)/S cell cycle progression in gastric cancer cells. *World J Gastrointest Oncol*. 2011;3:119-122.
- Miyazaki H, Shiozaki A, Niisato N, et al. Chloride ions control the G1/S cell-cycle checkpoint by regulating the expression of p21 through a p53-independent pathway in human gastric cancer cells. *Biochem Biophys Res Commun*. 2008;366:506-512.
- Shiozaki A, Miyazaki H, Niisato N, et al. Furosemide, a blocker of Na⁺/K⁺/2Cl⁻ cotransporter, diminishes proliferation of poorly differentiated human gastric cancer cells by affecting G0/G1 state. *J Physiol Sci*. 2006;56:401-406.

26. Iitaka D, Shiozaki A, Ichikawa D, et al. Blockade of chloride ion transport enhances the cytotoxic effect of hypotonic solution in gastric cancer cells. *J Surg Res*. 2012;176:524-534.
27. James DB, Mary KG, Christian W. *International Union Against Cancer (UICC) TNM Classification of Malignant Tumors*, 8th edn. New York: Wiley; 2017.
28. Rock JR, Harfe BD. Expression of TMEM16 paralogs during murine embryogenesis. *Dev Dyn*. 2008;237:2566-2574.
29. Katoh M, Katoh M. Identification and characterization of human TP53I5 and mouse Tp53i5 genes in silico. *Int J Oncol*. 2004;25:225-230.
30. Liu Z, Zhang S, Hou F, Zhang C, Gao J, Wang K. Inhibition of Ca(2+) -activated chloride channel ANO1 suppresses ovarian cancer through inactivating PI3K/Akt signaling. *Int J Cancer*. 2019;144:2215-2226.
31. Bill A, Gutierrez A, Kulkarni S, et al. ANO1/TMEM16A interacts with EGFR and correlates with sensitivity to EGFR-targeting therapy in head and neck cancer. *Oncotarget*. 2015;6:9173-9188.
32. Song Y, Gao J, Guan L, Chen X, Gao J, Wang K. Inhibition of ANO1/TMEM16A induces apoptosis in human prostate carcinoma cells by activating TNF-alpha signaling. *Cell Death Dis*. 2018;9:703.
33. Keir ME, Butte MJ, Freeman GJ, Sharpe AH. PD-1 and its ligands in tolerance and immunity. *Annu Rev Immunol*. 2008;26:677-704.
34. Garcia-Diaz A, Shin DS, Moreno BH, et al. Interferon receptor signaling pathways regulating PD-L1 and PD-L2 expression. *Cell Rep*. 2017;19:1189-1201.
35. Andzinski L, Spanier J, Kasnitz N, et al. Growing tumors induce a local STING dependent Type I IFN response in dendritic cells. *Int J Cancer*. 2016;139:1350-1357.
36. Le DT, Durham JN, Smith KN, et al. Mismatch repair deficiency predicts response of solid tumors to PD-1 blockade. *Science*. 2017;357:409-413.
37. Hause RJ, Pritchard CC, Shendure J, Salipante SJ. Classification and characterization of microsatellite instability across 18 cancer types. *Nat Med*. 2016;22:1342-1350.
38. Ock C-Y, Keam B, Kim S, et al. Pan-cancer immunogenomic perspective on the tumor microenvironment based on PD-L1 and CD8 T-cell infiltration. *Clin Cancer Res*. 2016;22:2261-2270.
39. Kulangara K, Zhang N, Corigliano E, et al. Clinical utility of the combined positive score for programmed death ligand-1 expression and the approval of pembrolizumab for treatment of gastric cancer. *Arch Pathol Lab Med*. 2019;143:330-337.
40. Shang LI, Hao J-J, Zhao X-K, et al. ANO1 protein as a potential biomarker for esophageal cancer prognosis and precancerous lesion development prediction. *Oncotarget*. 2016;7:24374-24382.
41. He Y, Li H, Chen Y, et al. Expression of anoctamin 1 is associated with advanced tumor stage in patients with non-small cell lung cancer and predicts recurrence after surgery. *Clin Transl Oncol*. 2017;19:1091-1098.
42. Wu H, Guan S, Sun M, et al. Ano1/TMEM16A overexpression is associated with good prognosis in PR-positive or HER2-negative breast cancer patients following tamoxifen treatment. *PLoS One*. 2015;10:e0126128.
43. Zhao JJ, Zhou ZQ, Wang P, et al. Orchestration of immune checkpoints in tumor immune contexture and their prognostic significance in esophageal squamous cell carcinoma. *Cancer Manag Res*. 2018;10:6457-6468.
44. Wang H, Yao H, Li C, et al. PD-L2 expression in colorectal cancer: Independent prognostic effect and targetability by deglycosylation. *Oncoimmunology*. 2017;6:e1327494.
45. Seo AN, Kang BW, Kwon OK, et al. Intratumoral PD-L1 expression is associated with worse survival of patients with Epstein-Barr virus-associated gastric cancer. *Br J Cancer*. 2017;117:1753-1760.

SUPPORTING INFORMATION

Additional supporting information may be found online in the Supporting Information section.

How to cite this article: Katsurahara K, Shiozaki A, Kosuga T, et al. ANO9 regulates PD-L2 expression and binding ability to PD-1 in gastric cancer. *Cancer Sci*. 2021;112:1026-1037. <https://doi.org/10.1111/cas.14796>